Experimental Thermal and Fluid Science 97 (2018) 417–430

Contents lists available at ScienceDirect

Experimental Thermal and Fluid Science

journal homepage: www.elsevier.com/locate/etfs

Experimental study of subcooled flow boiling heat transfer on micro-pin-finned surfaces in short-term microgravity

Yonghai Zhang[a], Bin Liu[a], Jianfu Zhao[b,d], Yueping Deng[c], Jinjia Wei[a,c,*]

[a] School of Chemical Engineering and Technology, Xi'an Jiaotong University, Xi'an 710049, China
[b] CAS Key Laboratory of Microgravity, Institute of Mechanics, Chinese Academy of Sciences, Beijing 100190, China
[c] State Key Laboratory of Multiphase Flow in Power Engineering, Xi'an Jiaotong University, Xi'an 710049, China
[d] School of Engineering Science, University of Chinese Academy of Sciences, 19A Yuquan Rd, Beijing 00049, China

ARTICLE INFO

Keywords:
Microgravity
Flow boiling
Micro-pin-fins
Heat transfer
Critical heat flux

ABSTRACT

The flow boiling heat transfer of subcooled air-dissolved FC-72 on micro-pin-finned surfaces was studied in microgravity by utilizing the drop tower facility in Beijing. The micro-pin-fins with the dimension of $30 \times 30 \times 60\ \mu m^3$ (width × thickness × height), named PF30-60, were fabricated on a silicon chip by using the dry etching technique. For comparison, experiments of flow boiling heat transfer in terrestrial gravity were also conducted. The effects of inlet velocity on both flow boiling heat transfer and bubble behavior were explored. It was found that gravity has nearly no effect on flow boiling heat transfer for the departure of the inertial-force-dominant bubbles in the low and moderate heat fluxes regions. In contrast, in the high-heat-flux region, the flow boiling heat transfer deteriorates and the critical heat flux (CHF) decreases due to the bubble accumulation in the channel. For PF30-60 at $V = 0.5$ m/s, the CHF point can be inferred to be between 20.8 and 24.5 W/cm^2, which is 63.0–74.2% of that in normal gravity. Regarding PF30-60 at $V = 1.0$ m/s, the CHF point can be inferred to be between 25.4 and 31.6 W/cm^2, which is 67.6–84.0% of that in normal gravity. The impact of gravity on CHF is closely linked to the channel geometry parameter and surface modification. The dimensionless numbers, *Ch* (Channel number) and *Sf* (Surface number), were proposed to describe the effect of the channel geometry and surface modification on the ratio of CHF in microgravity to that in normal gravity ($CHF_{\mu g}/CHF_{1g}$). An empirical correlation based on *We* (Weber number), *Ch* and *Sf* was proposed to predict the value of $CHF_{\mu g}/CHF_{1g}$ ratio in good agreement with the experimental data. This study provides a new perspective to determine the threshold inlet velocity of inertial-force-dominant flow boiling under different experimental conditions at different gravity levels.

1. Introduction

The thermal management system in aerospace equipment, especially for the microelectronic device heat dissipation, requires the cooling system to be efficient and compact in its structure, and consume a low amount of energy. Phase change heat transfer with high heat flux, small heat dissipation area, and low working temperature, is a very efficient method compared with the single-phase heat transfer. Until now, many experimental studies on passive technologies, such as mixture fluid [1], nanofluids [2–5], surface modification [6,7], and simulation work [8] in relation to passive technologies have been performed to enhance pool boiling heat transfer. Meanwhile, pool boiling in different gravity conditions has been investigated in the last decade by numerous researchers [9–15], and there are many review papers regarding pool boiling in microgravity [16–20].

As is known, flow boiling can be a practical and effective method to prevent the formation of massive bubbles by liquid inertia to flush discrete bubbles away from the heated wall and sustain liquid replenishment of the heated wall. However, the flow boiling and vapor-liquid two-phase flow involve much more complicated mechanisms than that of the pool boiling, and only a few reports on flow boiling heat transfer in microgravity are available [21].

In previous studies over last several decades, the bubble dynamics and two-phase flow characteristics at low inlet velocities were the main aspects considered. Ma and Chung [22,23] studied the bubble dynamics of flow boiling in microgravity at the inlet velocity $V = 0$–0.3 m/s, and found that the bubble departure diameter deceases with increasing inlet velocity, indicating the influence of gravity level diminishes with increasing inlet velocity. The results of Saito et al. [24] indicated that the bubbles are difficult to detach from the heater, and merge to form much

* Corresponding author at: School of Chemical Engineering and Technology, Xi'an Jiaotong University, Xi'an 710049, China.
E-mail address: jjwei@mail.xjtu.edu.cn (J. Wei).

https://doi.org/10.1016/j.expthermflusci.2018.05.003
Received 3 February 2018; Received in revised form 27 April 2018; Accepted 6 May 2018
Available online 19 May 2018
0894-1777/

Nomenclature

b	width of heater (mm)
Bo	Boiling number, $Bo = q/Gh_{fg}$
Ch	channel number
c_{pl}	specific heat capacity of liquid, $J{\cdot}kg^{-1}{\cdot}K^{-1}$
CHF	critical heat flux (W/cm^2)
D_h	hydraulic diameter (mm)
Eo	Eötvös number
g	gravitational acceleration (m/s^2)
g_0, $1g$	earth gravity level (m/s^2)
G	mass velocity ($kg/m^2{\cdot}s$)
h	channel height (mm)
h_v	heat transfer coefficient, $W{\cdot}m^{-2}{\cdot}K^{-1}$
h_{fg}	latent heat of evaporation, kJ/kg
I_H	heating current (A)
K	$CHF_{\mu g}/CHF_{1g}$ of pool boiling
L	length of heater (mm)
L_c	capillary length (mm)
Nu	Nusselt number, $Nu = h_v D_h/\lambda_l$
p_h	heated perimeter (mm)
p_w	wetted perimeter (mm)
q	heat flux (W/cm^2)
Q_v	volume flow rate (m^3/s)
R_1, R_2	resistance (kΩ)
Re	Reynolds number, $Re = \rho_l V D_h/\mu$
Sf	surface number
t	time (s)
T_1, T_2, T_3, T_4	wall temperatures (°C)
T_a	average wall temperature (°C)
T_f	liquid temperature (°C)
T_{sat}	saturation temperature (°C)
U_H	heating voltage (V)
V	inlet liquid velocities (m/s)
w	width of channel (mm)
We	Weber number
ΔP	pressure drop (kPa)
ΔT_{sat}	wall superheat = $T_w - T_{sat}$ (K)
ΔT_{sub}	fluid subcooling = $T_{sat} - T_b$ (K)
μg	gravitational acceleration in microgravity (m/s^2)

Greek symbol

μ	dynamic viscosity, $N{\cdot}s{\cdot}m^{-2}$
λ_l	thermal conductivity of liquid, $W{\cdot}m^{-1}{\cdot}K^{-1}$
ρ_l	liquid density, $kg{\cdot}m^{-3}$
ρ_g	vapor density, $kg{\cdot}m^{-3}$
σ	surface tension (N/m)

larger bubbles along the heater rod in microgravity. The influence of the gravity level became more remarkable under the conditions at lower inlet fluid velocity, higher heat flux and lower inlet fluid subcooling. The two-phase flow pattern in a circular tube at microgravity level, including bubbly flow, slug flow and annular flow, is simpler than that in normal gravity in the absence of buoyancy. Celata et al. [25] studied the flow patterns in pipe flow boiling under microgravity conditions, and observed two typical flow patterns, bubbly flow, and intermittent flow. Narcy et al. [26] investigated forced convective boiling and vapor-liquid two-phase flow pattern at different gravity levels. The authors observed annular flow, slug flow and bubbly flow, and found that the gravity level has little impact on the flow for mass velocity larger than 400 $kg/m^2{\cdot}s$ regardless of the flow pattern. Zhao et al. [27,28] experimentally investigated two-phase gas-liquid flow. They proposed and modified the semi-theoretical Weber number model to improve the accuracy of prediction of the slug-to-annular flow transition of gas-liquid two-phase flow in microgravity.

Obviously, the absence of gravity deteriorates the performance of flow boiling heat transfer, because the bubble departure becomes more difficult and the bubble emerging phenomenon becomes much more dramatically. Regarding the heat transfer coefficient at low and moderate heat fluxes in microgravity, there is a disagreement among different experiments. Baltis et al. [29] found that the heat transfer performance is enhanced at low mass velocity in microgravity compared with that of in normal gravity, and that this tendency becomes less obvious with increasing mass velocity. The results of Luciani et al. [30,31] indicated that the flow boiling heat transfer coefficient in a minichannel is enhanced in microgravity. In contrast, Ohta [32] and Ma and Chung [33] found that the heat transfer coefficient is decreased in microgravity. However, instead of the disagreement in heat transfer coefficient, the influence of gravity is definitely weakened with increasing mass velocity. Therefore, it is very important for space instruments to find the threshold of velocity at different gravity levels.

The critical heat flux (CHF) is also an important parameter for boiling heat transfer to prevent the burnout of electronic devices. Ohta [32] obtained limited flow boiling critical heat flux data in microgravity at high inlet quality, but noted that they could not measure CHF accurately in the absence of local wall temperature measurements along the heated wall. Ma and Chung [33] investigated the subcooled flow boiling of FC-72 across a heated 0.254 mm platinum wire by a 2.1 s drop tower. They found that the CHFs significantly decline in microgravtiy. However, the differences in both the heat transfer rate and CHF between microgravity and normal gravity decrease with increasing flow rate. Zhang et al. [34] tested a series of CHFs at different inlet liquid velocities under normal gravity and microgravity conditions. They found that the CHF in microgravity dramatically declines at low inlet liquid velocities compared with that in normal gravity. The effect of gravity on CHF is weaker as the inlet velocity increases. When the inlet liquid velocity exceeds 1.5 m/s, the influence of gravity almost vanishes and flow boiling is inertial-force-dominant. Konishi et al. [35,36] conducted the flow boiling experiments in a rectangular channel fitted with two opposite heating walls at the liquid inlet velocities of 0.1–1.9 m/s, and found that the enhancement in flow boiling heat transfer increases with increasing gravity level, whereas reduces with increasing microgravity level. This observation is similar to the results of others aforementioned. They also discovered that double-sided heating can achieve better heat transfer performance compared with that of single-sided heating at the same inlet velocities and heat fluxes. Konishi and Mudawar [37] summarized the research results regarding flow boiling and CHF in microgravity, and noted that the work of experimental investigation, correlations, mechanistic and computational models are still lacking for the application of flow boiling in future space systems.

From the previous literature review, it can be found that the research data of flow boiling heat transfer performance, especially for CHF in microgravity, is extremely lacking. As we know, the CHF of flow boiling is affected by many factors, such as inlet velocity and channel geometry parameter [38]. In addition, the experimental results of pool boiling on a smooth silicon chip and a micro-pin-finned chip in microgravity conducted by Xue et al. [39,40] and Zhang et al. [41] indicated that the CHF can be improved significantly due to the existence of micro-pin-finned structures. Therefore, surface modification is also an important factor influencing the CHF in microgravity. Based on the cooling requirement of electronic device in the future space equipment, the purposes of this paper are listed as follows:

(1) To investigate the flow boiling heat transfer on micro-pin-finned surfaces at different gravity levels.
(2) To study the influences of inlet liquid velocity, channel geometry and surface modification on the CHF of flow boiling at different gravity levels.

2. Experimental apparatus and test procedures

2.1. Experimental apparatus

The flow boiling heat transfer test facility system is presented schematically in Fig. 1. The test system comprises the pipeline system, testing section, data acquisition and visualization system. For the pipeline system, the working fluid (FC-72, T_{sat} = 56 °C) was pumped by a mini pump. The volume flow rate (Q_v), which was measured by a turbine flowmeter (ZHLW-6 0–600 L/h), was adjusted by a potentiometer. A differential pressure transmitter (ZHDP600 0–10 kPa) was fixed on the testing section for the pressure-drop (ΔP) measurement. To obtain a relatively stable pressure drop, the pressure taps were set at the upstream and downstream of heater with distances of 57 mm and 55 mm, respectively. In order to maintain the pressure at atmospheric pressure, a rubber bag was attached to a tank with a capacity of 2 L. In this study, the liquid subcooling (ΔT_{sub}) is approximately 15 K (which was sustained by an auxiliary heater, a condenser, and a PID temperature controller), and the liquid temperature (T_f) was measured by a platinum resistance thermometer (Pt-100A).

The test section with a size of 545 × 80 × 43 mm^3 was made of polycarbonate to allow visualization. The flow boiling heat transfer occurred in a rectangular channel with the cross-sectional dimensions of 12 × 3 mm^2. The heater, with dimensions of 40 × 10 × 0.5 mm^3 (length × width × thickness), was combined with two silicon chips with the dimensions of 20 × 10 × 0.5 mm^3. The distance from the heater to the inlet of rectangular channel is 60 times greater than the hydraulic diameter (D_h = 4.8 mm). Therefore, the flow state on the heater can be regarded as fully developed turbulent flow. The micro-pin-fins with the dimensions of 30 × 30 × 60 μm^3 (width × thickness × height), named PF30-60 (as shown in Fig. 2), were fabricated on a silicon chip by using the dry etching technique. Our group [42–44] has made noticeable progress in nucleate boiling enhancement by use of micro-pin-fins (10–50 μm in thickness and 60–270 μm in height) which were fabricated on silicon surface by the dry etching technique. After series of experiments were conducted to study the size effects of micro-pin-fin, the results showed that the fin spacing ranging from 30 to 50 μm and fin height ranging from 60 to 200 μm were preferable alternatives for the design of micro-fin-finned surfaces in the enhancement of nucleate boiling heat transfer. Moreover, micro-pin-fins with the thickness and spacing of 30 μm always showed higher CHF than that of 50 μm with the same height. Thus, the micro-pin-finned surfaces with the thickness of 30 μm and height of 60 μm were selected. In this

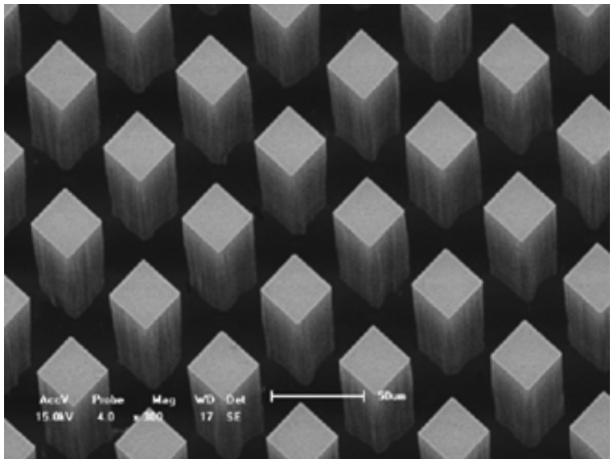

Fig. 2. SEM image of PF30-60.

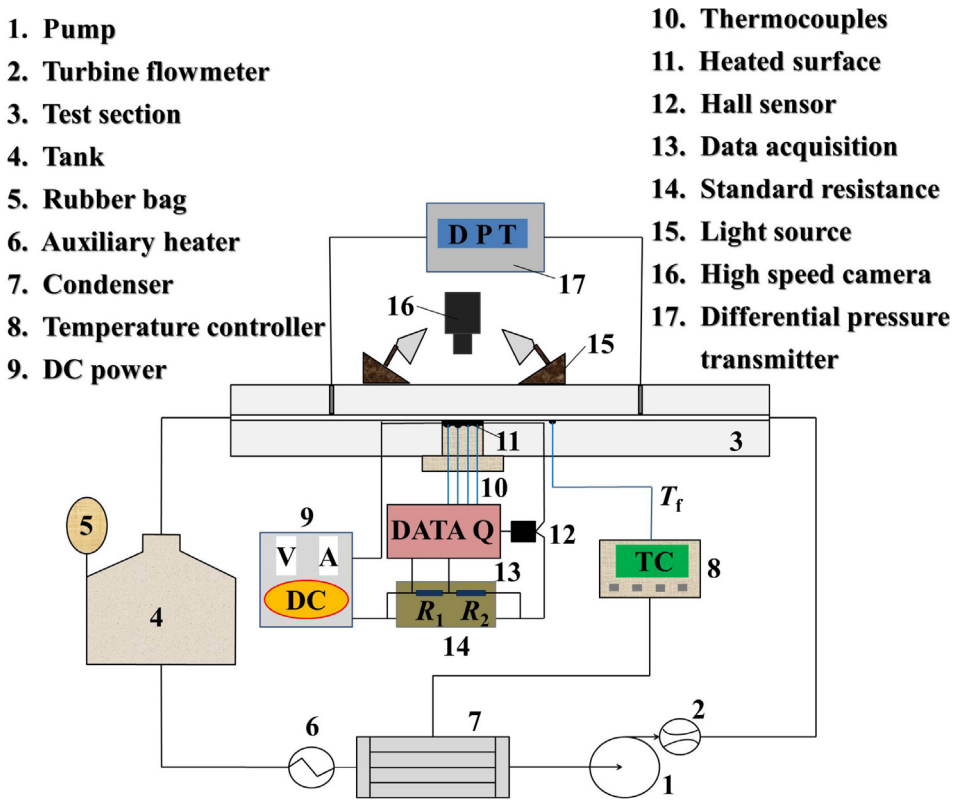

Fig. 1. Schematic diagram of the experimental apparatus.

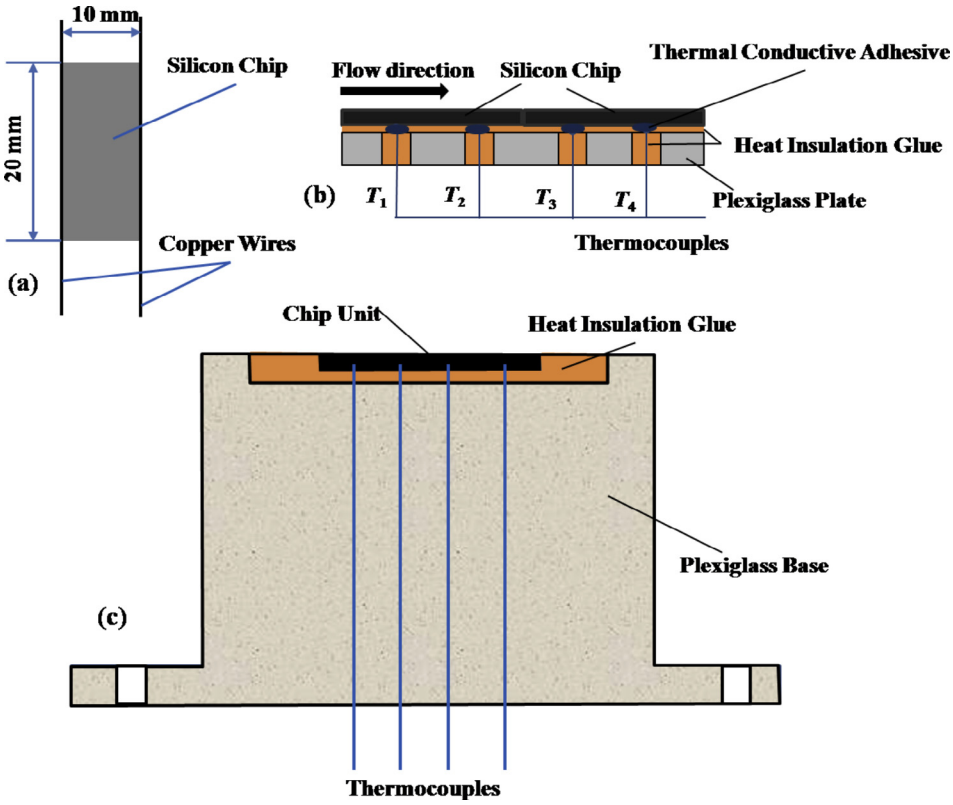

Fig. 3. Schematic diagram of the test section: (a) Test chip soldering, (b) Chip unit, and (c) Chip heating module.

experiment, the heater was based on Joule heating under the application of DC power. As illustrated in Fig. 3(a), the silicon chip was connected to a programmable DC power supply by using two 0.25 mm diameter copper wires that were soldered to the side surfaces of test chip at the opposite ends by using ultrasonic bonding method. Fig. 3(b) shows the details of chip unit. Four 0.15 mm diameter T-type thermocouples for wall temperature measurements were attached to the back of the test chip by thermal conductive adhesive, and separated by the same distance of 10 mm. The test chip was bonded onto a plexiglass plate by using adhesive with heat insulating glue to minimize heat loss. Next, the chip unit was packaged in the plexiglass base by using a thicker layer of heat insulation glue [as shown in Fig. 3(c)]. Therefore, it can be considered that the heat transfer only occurs effectively on the upper surface of the test chip.

A high-speed digital camera (VITcam CTC) with a lens (ComputarMLM-3XMP) operating at 1000 frames per second and a resolution of 512 × 1280 pixels was used for visualization. Simultaneously, four 25-Hz CCD cameras were installed in front of the display panel of turbine flowmeter, differential pressure transmitter, high-speed camera and temperature controller to monitor the operational state of the test system. Two standard resistances in series (R_1 = 5 kΩ and R_2 = 100 kΩ) connected to the test chip in parallel were used to measure the heating voltage (U_H) across the silicon chip in the circuit, and the heating current (I_H) through the silicon chip was measured by a hall senor. The gravity level was obtained by a gravity acceleration sensor. Ultimately, the wall temperature (T_1–T_4), the pressure drop (ΔP), the heating voltage (U_H) and the heating current (I_H) were transmitted to a data acquisition system (DI710-UHS).

2.2. Test procedures

In the present study, FC-72 was chosen as the working fluid without degasification processing because a previous study [41] proved that the existence of non-condensable gas merely influences the onset of nucleate boiling, whereas the heat fluxes of this study are much higher than that at the onset of nucleate boiling. Two inlet liquid velocities (V = 0.5 and 1.0 m/s, corresponding the mass velocity (G) of 815.7 and 1631.4 kg/m^2·s, respectively) were chosen. The flow boiling heat transfer and bubble behavior on heated micro-pin-finned surfaces as well as on a smooth surface (Chip S) were studied in microgravity by utilizing the drop tower facility in the CAS Key Laboratory of Microgravity. The microgravity level (μg) is approximately 10^{-2} to 10^{-3} g_0 in the free-falling period, where g_0 is gravitational acceleration in terrestrial condition. The working fluid in the pipeline was heated to 41 °C before the test chip was heated. Next, the test chip was heated under a set constant input voltage to initiate boiling on the heater wall in terrestrial gravity before the release of drop capsule, and the heat transfer reached a steady state after 2.5 min approximately. Afterwards, the drop capsule was released to achieve a 3.6 s effective microgravity environment. During the process, the bubble behavior on the heated surface was captured by the high-speed camera before and after the release of the drop capsule for 4.096 s. The period of observation was divided into two parts according to the gravity acceleration signal: the first section (0.205 s) is in terrestrial gravity before release, whereas the second section (3.891 s) is in microgravity after release. Note that the experiment for each heat flux was conducted only one test run because of the limitation of experimental resources. To ensure the reproducibility and reliability of the experimental data, experiments of flow boiling heat transfer in terrestrial gravity were also conducted for comparison. Tables 1 and 2 show the detailed experimental conditions of PF30-60 in microgravity at

Table 1
Experimental conditions of PF30-60 in microgravity at V = 0.5 m/s.

Run#	Subcooling ΔT_{sub} (K)	Heating Voltage U_H (V)	Heating current I_H (A)	Heat flux q (W/cm^2)	Pressure P_s (kPa)
1#	14.5	19.6	1.42	6.9	103.4
2#	15.0	29.7	1.95	14.5	100.4
3#	14.9	35.4	2.36	20.9	100.8
4#	14.5	37.0	2.66	24.5	100.7

Table 2
Experimental conditions of PF30-60 in microgravity at $V = 1.0$ m/s.

Run#	Subcooling ΔT_{sub} (K)	Heating Voltage U_H (V)	Heating current I_H (A)	Heat flux q (W/cm^2)	Pressure P_s (kPa)
1#	14.8	23.5	1.73	10.2	103.4
2#	15.0	33.3	2.35	19.6	101.5
3#	15.1	39.6	2.57	25.4	102.8
4#	14.9	42.4	2.98	31.6	100.7

$V = 0.5$ m/s and $V = 1.0$ m/s, respectively. In the present study, in order to attain CHF in microgravity, the heating method with constant heating voltage was used. For the silicon chip, CHF will lead to an obvious increase of the heater surface temperature. Meanwhile, the resistance of chip increases and the corresponding heating current decreases. Thus, from the curves of wall temperature and heating current, we can identify the CHF point.

For validating the experimental setup, we compared our boiling curves of smooth surface at $V = 0.5$ m/s in normal gravity with the literatures [45,46]. As shown in Fig. 4, it can be seen that our results show heat transfer deterioration compared to the results of Rainey et al. [45] due to small liquid subcooling, and better heat transfer performance than that of Chang et al. [46] due to large liquid subcooling and inlet velocity. Besides, our results show good repeatability.

2.3. Uncertainty analysis

In this study, the uncertainty of platinum resistance thermometer is 0.23 °C. As shown in Tables 1 and 2, the maximum experimental operation error of liquid temperature is 0.5 °C. The temperature of the working liquid is 40.5 °C. Therefore, the uncertainty of liquid temperature is 1.4%. In addition, the error of the wall temperature of the heater is 0.3 °C, and its uncertainty is approximately 0.73%. The input heat flux of heater can be calculated as

$$q = \frac{U_H \cdot I_H}{L \cdot b} \tag{1}$$

where L and b represent the length and width of heater, respectively. The uncertainty of input heat flux (Δq) mainly originates from the uncertainty of the heating voltage and the heating current as well as the tolerance of silicon chip manufacturing. The uncertainty of heat flux can be calculated as

$$\frac{\Delta q}{q} = \left(\left(\frac{\Delta U_H}{U_H}\right)^2 + \left(\frac{\Delta I_H}{I_H}\right)^2 + \left(\frac{\Delta L}{L}\right)^2 + \left(\frac{\Delta b}{b}\right)^2\right)^{1/2} \tag{2}$$

where ΔU_H, ΔI_H, ΔL, and Δb are the error of the heating voltage, the heating current, the length of the heater and the width of the heater, respectively. In this article, the measurement uncertainties for $\Delta U_H/U_H$, $\Delta I_H/I_H$, $\Delta L/L$, and $\Delta b/b$ are 0.1%, 0.014%, 0.5% and 0.5%, respectively. The total heat loss Δq_{tot} comprises the uncertainty of the input heat flux (Δq), the heat loss through substrate conduction (Δq_{con}) and the heat loss of the fluctuation of volume flow rate (Δq_V). The uncertainty of total ratio of heat loss is calculated as

$$\frac{\Delta q_{tot}}{q} = \frac{\Delta q}{q} + \frac{\Delta q_{con}}{q} + \frac{\Delta q_V}{q} \tag{3}$$

According to the heat loss simulation results of O'connor and You [47], the ratio of heat loss through substrate conduction $\Delta q_{con}/q$ is approximately 5.0%. The fluctuation of the volume flow rate during the experiment (maximum fluctuation of volume flow rate is approximately 7%) can also influence the CHF. According to the experimental results in normal gravity, the uncertainty caused by the fluctuation of volume flow rate $\Delta q_V/q$ is approximately 0.8%. Thus, the uncertainty of heat flux is less than 7.0%.

3. Result and analysis

3.1. Heater wall temperatures and bubble behavior at different gravity levels

The wall temperatures and bubble behavior at different gravity levels and input heat fluxes with $V = 0.5$ m/s are shown in Fig. 5. The time entering microgravity condition was set to 0 s, and the flow boiling is in normal gravity when $t < 0$ and in microgravity when $t > 0$.

At input heat fluxes of $q = 6.9$ and 14.5 W/cm^2, according to the visualizations shown in Fig. 5(b) and (d), the heat transfer is in the nucleate boiling region, and the wall temperatures at different locations remain constant at different gravity levels as shown in Fig. 5(a) and (c). Compared with that in normal gravity, there is no obvious distinction in bubble behavior under microgravity, except the diameter of bubbles at the downstream is slightly larger than that in normal gravity. This occurs because it is difficult for the bubbles to depart but easier for them to coalesce in the absence of buoyancy. Similar phenomena were also reported in [24,25,48]. However, in this study, the mass velocity ($G = 815.7$ kg/m^2·s) is much higher than that reported in [24,25,48], and the inertial force is the dominant factor for the bubble departure. Therefore, the difference of bubble behavior is not so evident. When the input heat flux increases to 20.8 W/cm^2 [as shown in Fig. 5(e) and (f)], we found that the bubble behavior changes notably from the visualizations. A large bubble is formed at the downstream of the heater and occupies the entire cross-section of the channel in microgravity conditions, as denoted by the red outline in Fig. 5(f). Because the fluid inertial force is still larger than the resistance of this large confined bubble, the large confined bubble is formed and pushed away continuously. Moreover, the wall temperature downstream of the heater (T_4) is much higher than the temperature upstream, although the wall temperatures and the flow boiling still remain steady under this circumstance, as shown in Fig. 5(e). Under the condition of input heat flux of 24.5 W/cm^2 [as shown in Fig. 5(h)], many lager bubbles are formed at the downstream region at normal gravity level, as shown in the visualizations. The wall temperatures, T_3 and T_4, begin to increase at $t = 1.2$ and 1.9 s, respectively, as shown in Fig. 5(g). The visualization of $q = 24.5$ W/cm^2 at $t = 1.2$ s shows that the length of the confined bubble, as marked by the red outline in Fig. 5(h), is much longer than that of $q = 20.8$ W/cm^2. Moreover, although the confined bubble can be pushed away periodically, the length of the confined bubble increases gradually. Because the microgravity duration of each drop tower test is only 3.6 s, the vapor film does not occupy the entire heater, and the wall temperatures T_1 and T_2 do not exhibit an obvious increase. However, according to the trend of T_4 and T_3 shown in Fig. 5(g), the CHF has occurred at the downstream of the heater surface. Thus, it is

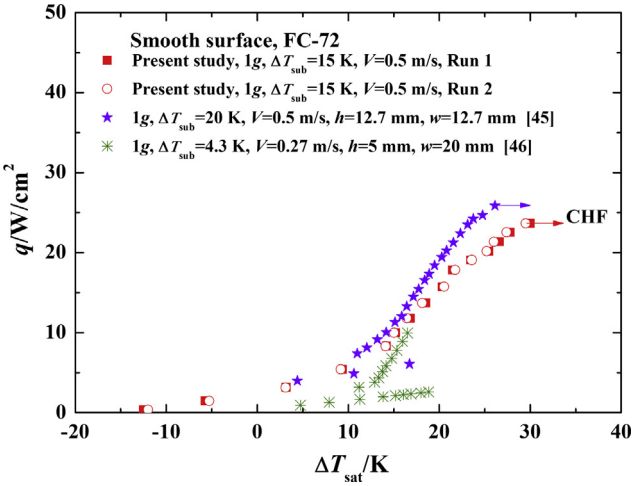

Fig. 4. Comparison between the results obtained in the present study with the literature [45,46]

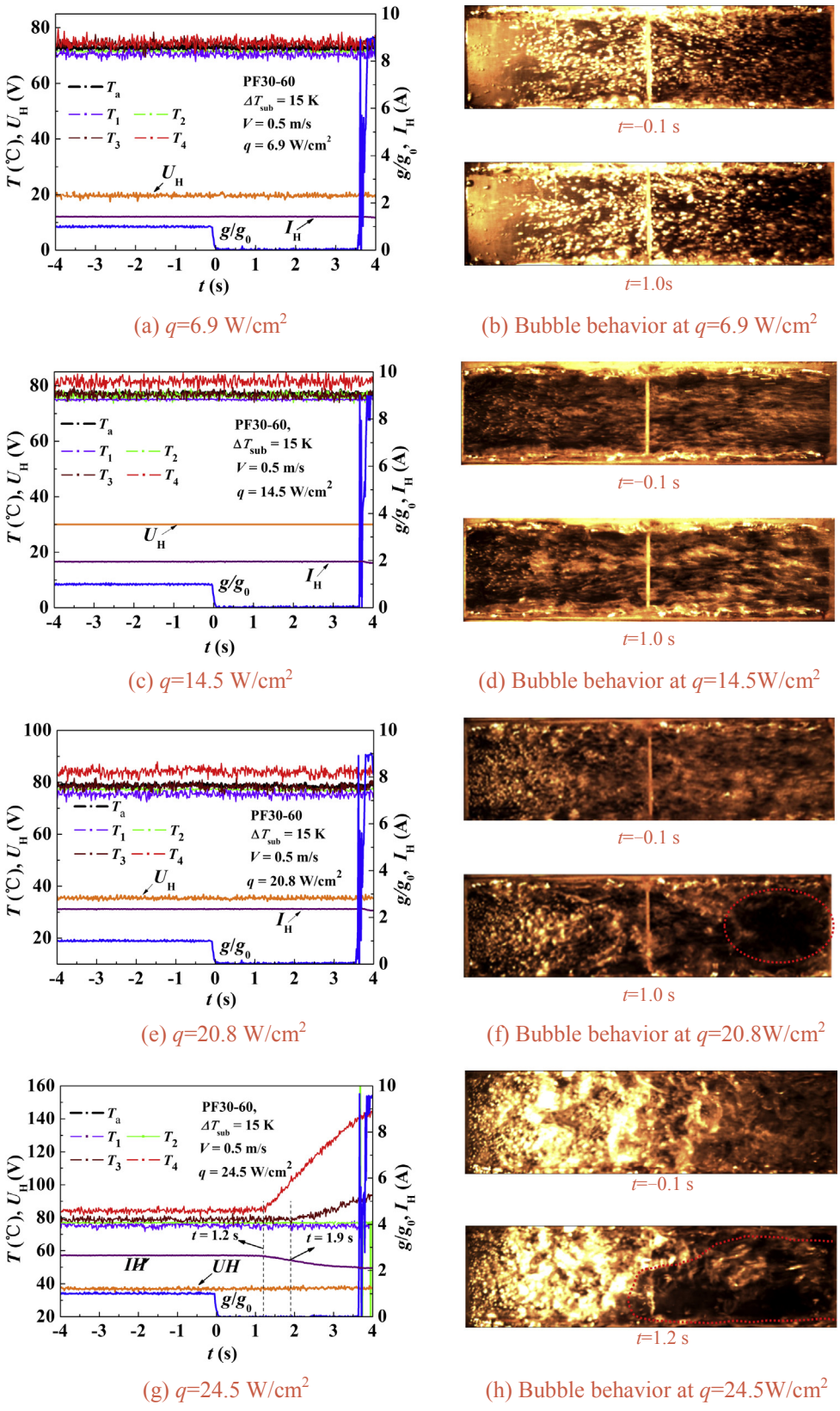

(a) q=6.9 W/cm² (b) Bubble behavior at q=6.9 W/cm²

(c) q=14.5 W/cm² (d) Bubble behavior at q=14.5W/cm²

(e) q=20.8 W/cm² (f) Bubble behavior at q=20.8W/cm²

(g) q=24.5 W/cm² (h) Bubble behavior at q=24.5W/cm²

Fig. 5. Wall temperatures and bubble behavior at different gravity levels at V = 0.5 m/s.

impossible to maintain a steady nucleate boiling state, and the nucleate boiling will be converted to film boiling at the upstream of the heater surface if the duration of microgravity is long enough. In addition, as mentioned above, the heating method with constant heating voltage was used in the present study. Thus, the heating voltage (U_H) in Fig. 5(a), (c), (e), and (g) remain constant in the entire heat transfer region. For steady heat transfer with q = 6.9, 14.5, and 20.8 W/cm², the heating currents (I_H) also remain constant. However, for

q = 24.5 W/cm^2, the heating current (I_H) begins to decrease, because the CHF has occurred, leading to an obvious increase of the heater surface temperature. As a result, the resistance of chip increases and the corresponding heating current decreases as shown in Fig. 5(g).

Regarding V = 1.0 m/s, similar to Fig. 5, the wall temperatures and bubble behavior at different gravity levels and input heat fluxes are shown in Fig. 6. As shown in Fig. 6(b), (d), and (f), no evident differences in bubble behavior are observed between the microgravity and normal gravity cases at q = 10.2, 19.6, and 25.4 W/cm^2, respectively, because, at V = 1.0 m/s, the inertial force plays a much more important role for bubble departure than at V = 0.5 m/s. Moreover, the wall temperatures remain steady at these three input heat fluxes as shown in Fig. 6(a), (c) and (e). Compared with the bubble behavior at V = 0.5 m/s (Fig. 5), with increasing inlet velocity, the influence of

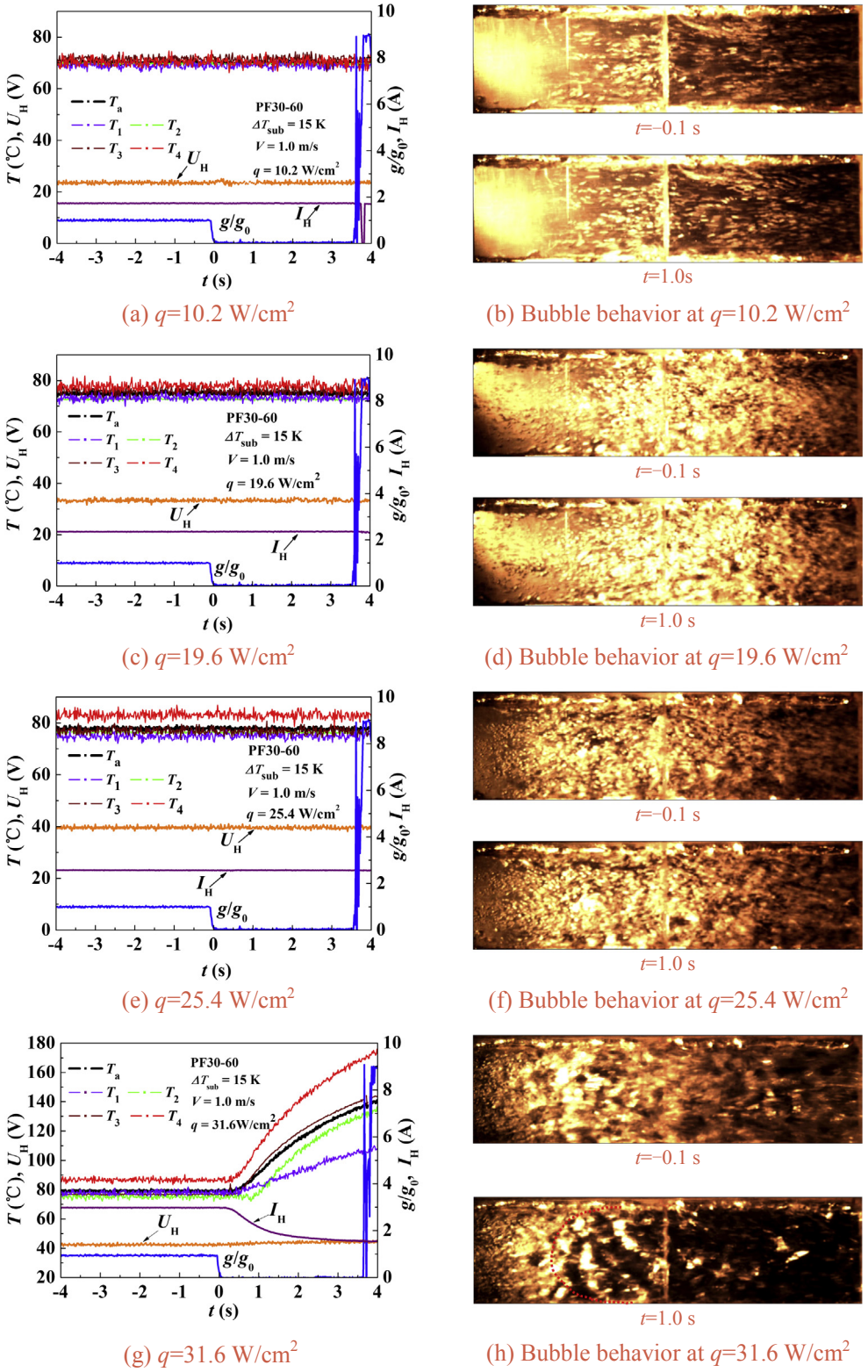

(a) q=10.2 W/cm^2 (b) Bubble behavior at q=10.2 W/cm^2

(c) q=19.6 W/cm^2 (d) Bubble behavior at q=19.6 W/cm^2

(e) q=25.4 W/cm^2 (f) Bubble behavior at q=25.4 W/cm^2

(g) q=31.6 W/cm^2 (h) Bubble behavior at q=31.6 W/cm^2

Fig. 6. Wall temperatures and bubble behavior in different gravity conditions at V = 1.0 m/s.

gravity on bubble behavior decreases. Similar phenomena were also observed in literatures [22,23,34], is attributed to the effect of buoyancy gradually receding and the inertial force becoming the dominant mechanism of flow boiling heat transfer with the inlet velocity increase. At the input heat flux of $q = 31.6\ W/cm^2$, a very rapid transition from nucleate boiling to film boiling can be observed in Fig. 6(h). All wall temperatures rise sharply after the flow boiling entering microgravity condition as shown in Fig. 6(g). Simultaneously, the flow pattern converted from bubbly flow to wavy flow.

3.2. Pressure drop

The pressure drop can also provide useful information for the flow boiling heat transfer and bubble behavior. Fig. 7 shows pressure drop as a function of time of Chip S and PF30-60 at different velocities. It can be seen that the pressure drop increases in microgravity, and the response times of the pressure-drop changes are different from each other at different heat fluxes and velocities. Furthermore, the pressure drop first increases and then decreases for all cases after completion of a flow cycle. Fig. 8 shows the average pressure drop of Chip S and PF30-60 with different input heat fluxes for different inlet liquid velocities in normal gravity and microgravity. It was found that ΔP increases significantly with increasing inlet velocity. In addition, the pressure drop increases with the augmentation of input heat flux in the nucleate boiling region; this observation is attributed to the increasing quality of vapor as the inlet heat flux increases. Sadaghiani and Koşar [49] have conducted numerical and experimental investigations on the effects of diameter and length on high mass flux subcooled flow boiling in horizontal microtubes, and they also found that the increase in wall heat flux can lead to an increase in both the two-phase frictional and accelerational components of pressure drop, resulting in an increasing trend with heat flux. Moreover, as the number of bubbles increases, the pressure drop increases.

From the comparison of the pressure drop under different gravity conditions, the pressure drop in microgravity is found to be higher than that in normal gravity for identical flow rate and heating conditions. Because it is difficult for the bubbles to depart in the absence of gravity, more energy is thus required to remove the bubbles from the heating surface. However, this tendency is not obvious when the same bubble behavior is obtained in normal gravity and microgravity. For $q = 20.8\ W/cm^2$ at $V = 0.5\ m/s$ of PF30-60, the pressure drop is much higher in microgravity than that in normal gravity because of the notable change of bubble behavior. This is because the drastic bubble coalescent and accumulation behavior resulting in an abrupt augmentation of the pressure drop. When $q = 31.6\ W/cm^2$ at $V = 1.0\ m/s$, $q = 24.5\ W/cm^2$ at $V = 0.5\ m/s$ of PF30-60, and $q = 21.3\ W/cm^2$ at $V = 0.5\ m/s$ of Chip S, the vapor fraction decreases quickly as the heat

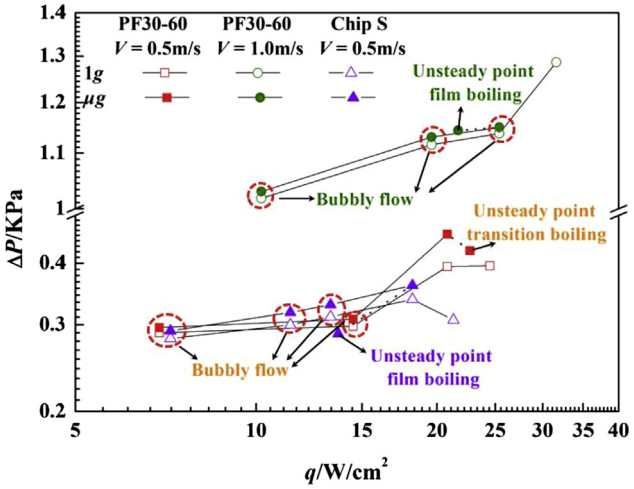

Fig. 8. Average pressure drop with different input heat fluxes at different gravity levels and inlet liquid velocities.

transfer in microgravity deteriorates rapidly, and the flow pattern changes from bubbly flow to wavy flow, causing further pressure drop. Besides, Chip S at $q = 7.2\ W/cm^2$ shows slight lower pressure-drop value than that of PF30-60 at $q = 6.9\ W/cm^2$ as shown in Fig. 8. This is because more bubbles were generated on the surface of PF30-60 compared with that of Chip S, as shown in Fig. 9(a) and (b). With increasing heat flux, Chip S at $q = 13.3\ W/cm^2$ shows slightly higher value than that of PF30-60 at $q = 14.5\ W/cm^2$ as shown in Fig. 8. It can be seen in Fig. 9(c) and (d) that the number of bubbles with PF30-60 is larger than that of Chip S, but the size of bubbles with PF30-60 is smaller than that of Chip S. However, PF30-60 at $q = 24.5\ W/cm^2$ shows an obvious pressure drop increment compared with that of Chip S at $q = 21.3\ W/cm^2$ as shown in Fig. 8. It is attributed that more bubbles were generated on the surface of PF30-60 due to high heat flux as shown in Fig. 9(e) and (f), and thus pressure drop increases.

3.3. Flow boiling curves and critical heat flux

To validate the reliability of the experimental system and confirm the heat flux range studied in microgravity conditions, a ground experiment was conducted with the same experimental installation as that of microgravity tests. The average wall temperature, T_a, is calculated as $(T_1 + T_2 + T_3 + T_4)/4$. Fig. 10 describes the boiling curves of PF30-60 at different gravity levels. The ΔT_{sat} represents wall superheat, which is the difference between T_a and T_{sat}. The heat flux is calculated by the heating voltage U_H and heating current I_H. It was found that the points

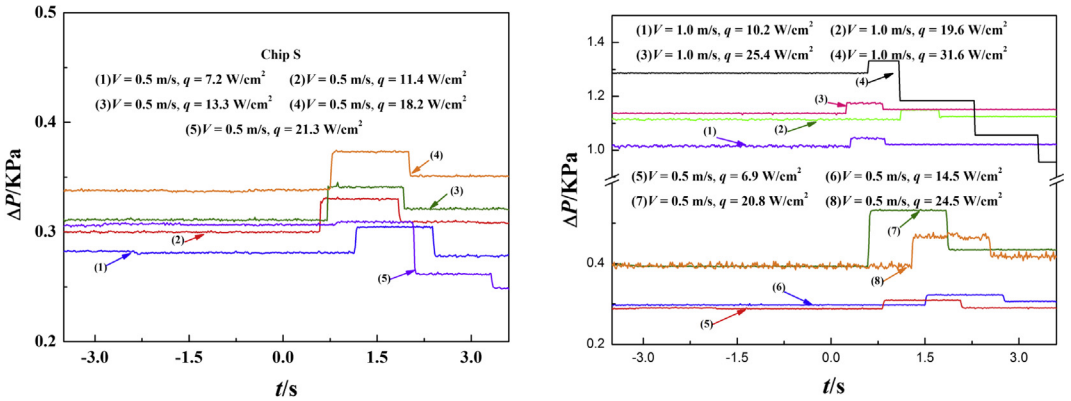

(a) Chip S (b)PF30-60

Fig. 7. Pressure drop as a function of time of Chip S and PF30-60.

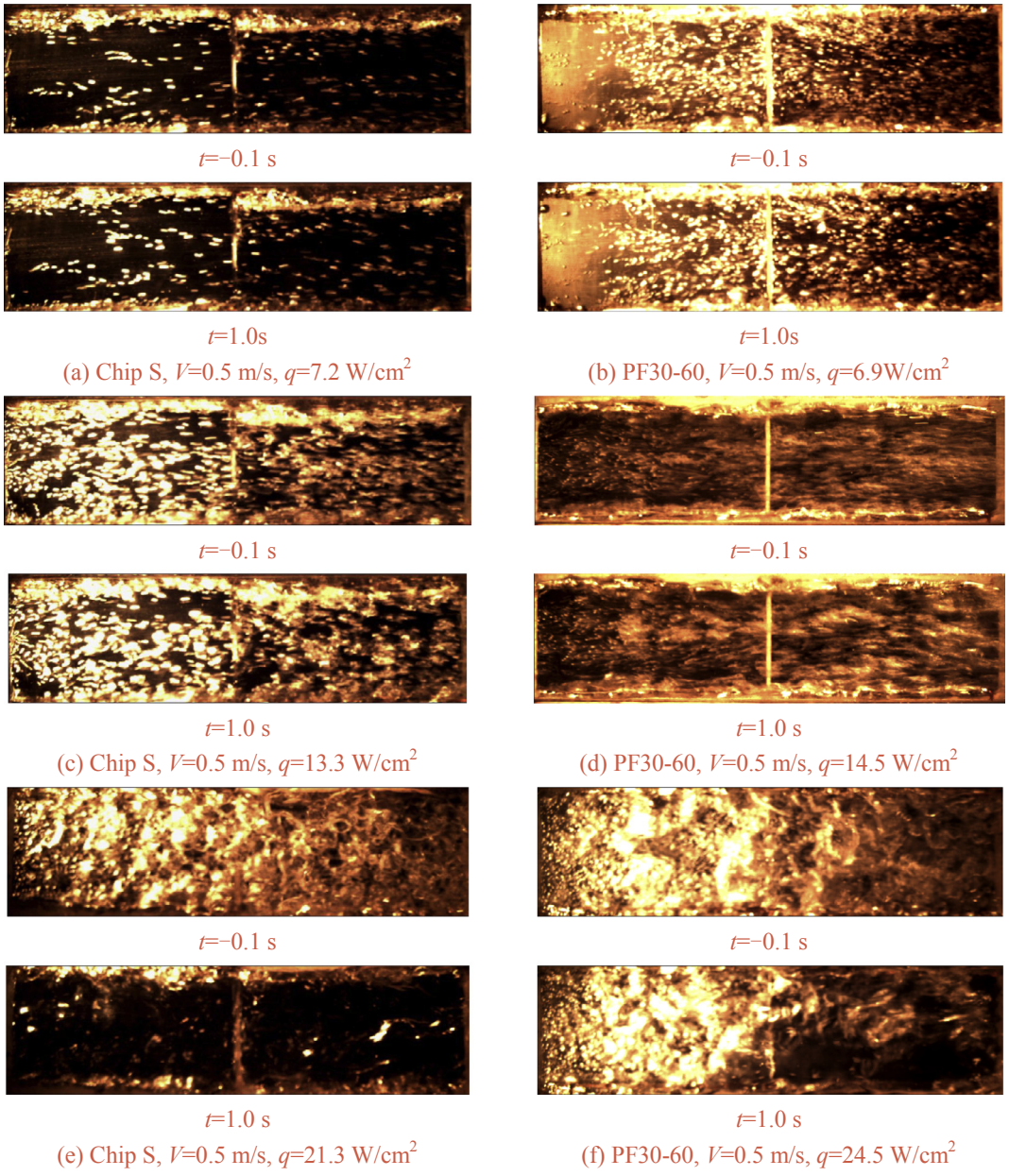

Fig. 9. Visualization images of Chip S and PF30-60 at different gravity levels at inlet velocity V = 0.5 m/s.

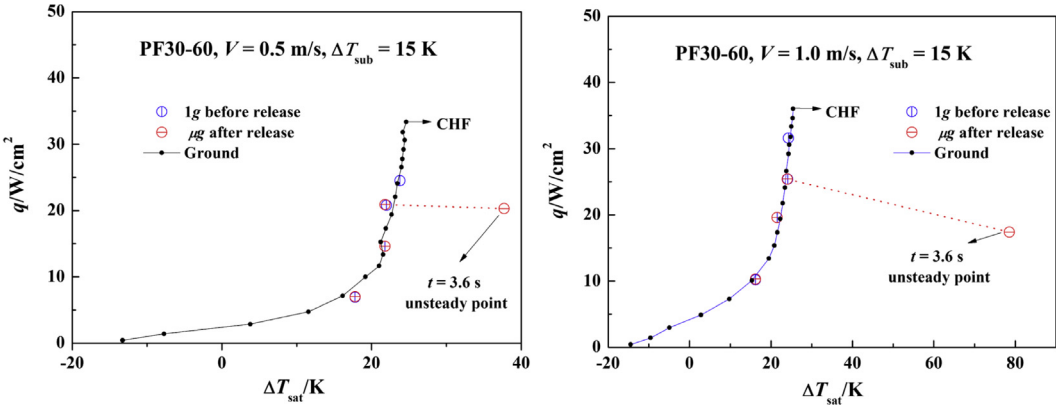

(a) V = 0.5 m/s (b) V = 1.0 m/s

Fig. 10. Flow boiling curves of PF30-60 at different gravity levels.

before release are in good agreement with the boiling curve obtained on the ground, thus proving the good repeatability and reliability of the data points.

It is obvious that the absence of gravity deteriorates the performance of flow boiling heat transfer in the high-heat-flux region, because the emerging bubble phenomenon becomes more vigorous in microgravity. In contrast, there is no obvious heat transfer performance difference between microgravity and terrestrial gravity except for CHF. As mentioned above, for the heat transfer coefficient at low and moderate heat fluxes in microgravity, although there is a disagreement among different experiments, the influence of gravity is certainly weakened as the mass velocity increases because the inertial force is dominant. In addition, the flow mass velocities are 815.7 and 1632 kg/m^2·s at low and moderate heat fluxes in the present study, respectively, which is much higher than that reported in [29–33]. Therefore, the lack of an obvious heat transfer performance distinction at low and moderate heat fluxes is reasonable.

From Fig. 11(a), in normal gravity, it can be seen that the largest heat transfer coefficient of Chip S is 5126 W·m^{-2}·K^{-1} at V = 0.5 m/s, and q = 18.2 W·cm^{-2}. For PF30-60, the largest heat transfer coefficients are 6314 W·m^{-2}·K^{-1} at V = 0.5 m/s with q = 24.5 W·cm^{-2} and 8040 W·m^{-2}·K^{-1} at 1.0 m/s with q = 31.6 W·cm^{-2}, respectively. In microgravity, the largest heat transfer coefficient of Chip S is 4986 W·m^{-2}·K^{-1} at V = 0.5 m/s, and q = 18.1 W·cm^{-2}. For PF30-60, the largest heat transfer coefficients are 5679 W·m^{-2}·K^{-1} at V = 0.5 m/s with q = 21.8 W·cm^{-2} and 6512 W·m^{-2}·K^{-1} at 1.0 m/s with q = 25.4 W·cm^{-2}, respectively. However, all the heat transfer coefficients remain constant at a fixed heat flux except for the unsteady points in microgravity. It is attributed that the inertial force still dominates the heat transfer process. Fig. 11(b) shows the comparison of predicted heat transfer coefficients and experimental data. The heat transfer coefficient correlation of Sun and Mishima [50] was used, and the correlation is shown as follows:

$$h_v = \frac{6Re_l^{1.05}\cdot Bo^{0.54}}{We_l^{0.191}\cdot(\rho_l/\rho_g)^{0.142}}\cdot\frac{\lambda_l}{D_h} \quad (4)$$

where $We_l = \rho_l V^2 D_h/\sigma$, $Re = \rho_l V D_h/\mu$, and $Bo = q/Gh_{fg}$. It can be seen that the Eq. (4) underestimates our experimental results, but most data (95%) were predicted within −35%. However, we found in the present study that the boiling number shows the same effect as the results of Sun and Mishima [50] on heat transfer coefficient. Thus, the correlation can be expressed as Eq. (5), and most data (95%) were predicted within ± 15%, as shown in Fig. 11(b).

$$h_v = \frac{6Re_l^{1.05}\cdot Bo^{0.56}}{We_l^{0.191}\cdot(\rho_l/\rho_g)^{0.142}}\cdot\frac{\lambda_l}{D_h} \quad (5)$$

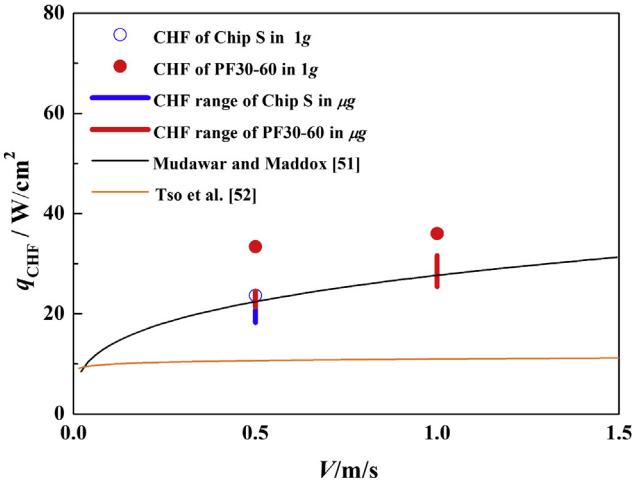

Fig. 12. Comparison of the experimental CHF with theoretically predicted values.

Fig. 12 shows a CHF comparison of chip S and PF30-60 at different gravity levels. The CHF of PF30-60 with inlet velocities of 0.5 and 1.0 m/s are 33.0 and 37.6 W/cm^2 under terrestrial gravity, respectively. However, we cannot capture the CHF point accurately in microgravity. For PF30-60, the highest heat flux conducted in microgravity is 24.5 W/cm^2 at V = 0.5 m/s. Obviously, it has reached CHF, and thus the CHF point can be inferred to be between 20.8 and 24.5 W/cm^2, which is 63.0–74.2% of that in normal gravity. Regarding PF30-60 at V = 1.0 m/s, using the same method, the CHF point can be inferred to be between 25.4 and 31.6 W/cm^2, which is 67.6–84% of that in normal gravity. Fig. 12 shows that CHF increases as the inlet velocity increases from 0.5 to 1.0 m/s in microgravity, in good agreement with the visualizations in Figs. 5 and 6. Moreover, the CHF of Chip S with an inlet velocity of 0.5 m/s is 23.2 W/cm^2 under terrestrial gravity, and the CHF under microgravity is between 18.2 and 21.3 W/cm^2 at V = 0.5 m/s, which is 78.4–91.8% of that in normal gravity. The CHF of PF30-60 is found to be slightly higher than that of Chip S at V = 0.5 m/s.

However, the ratio of CHF in microgravity to that in normal gravity ($CHF_{\mu g}/CHF_{1g}$) of PF30-60 is much lower than that of Chip S. In addition, the $CHF_{\mu g}/CHF_{1g}$ ratio of PF30-60 increases with increasing inlet velocity. The correlations of Mudawar and Maddox [51] and of Tso et al. [52] were used to predict our experimental results, and the correlations are shown in Eqs. (6) and (7), respectively.

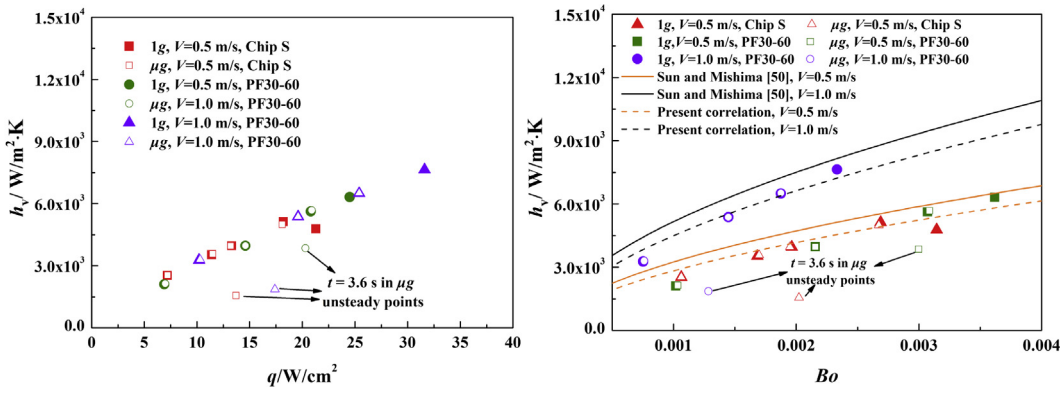

(a) h_v VS q (b) h_v VS Bo

Fig. 11. Comparison of the experimental heat transfer coefficient with theoretically predicted values.

$$q_{CHF} = 0.161\rho_g V h_{fg} We_2^{-8/23}\left(\frac{\rho_l}{\rho_g}\right)^{15/23}\left(\frac{L}{D_h}\right)^{1/23}\left(1+\frac{c_{pl}\Delta T_{sub}}{h_{fg}}\right)^{7/23}\left(1+0.021\frac{\rho_l}{\rho_g}\frac{c_{pl}\Delta T_{sub}}{h_{fg}}\right)^{16/23} \quad (6)$$

$$q_{CHF} = 0.203\rho_g V h_{fg} We_2^{-11/23}\left(\frac{\rho_l}{\rho_g}\right)^{15/23}\left(\frac{L}{D_h}\right)^{1/23}\left(1+\frac{c_{pl}\Delta T_{sub}}{h_{fg}}\right)^{7/23}\left(1+0.021\frac{\rho_l}{\rho_g}\frac{c_{pl}\Delta T_{sub}}{h_{fg}}\right)^{16/23} \quad (7)$$

where $We_2 = \rho_l V^2 L/\sigma$. In their correlations, they did not consider the effect of the gravity level. From Fig. 12, it can be seen that both correlations underestimate our experimental results. For the correlation of Tso et al. [51], it can only be used to predict CHF of flow boiling for $1 < We_2 < 1000$. However, We_2 is much larger than 1000 in the present study. So both correlations cannot be used to predict CHF of flow boiling in the present study.

Fig. 13(a)–(d) present a schematic of the liquid supply in the high-heat-flux region from different views. Regarding Chip S, the large bubble covers the heating surface and leads to the partial drying out of the heating surface, causing the heat transfer of the Chip S to deteriorate. Regarding PF30-60, fresh liquid can also be supplied to the heating surface by capillary force because of the existence of micro-channels on the micro-pin-finned surface. Therefore, good heat transfer performance is still exhibited in the high-heat-flux region. In our previous study on the pool boiling phenomena [43], it can be seen that the bubbles generate at the fin root at low heat flux, and then the small bubbles emerge from the gap between adjacent fins. The bubble continues to grow on the surface moving slowly upward. With increasing heat flux, small bubbles merge with the other adjacent bubbles to form larger ones. Near the CHF point, small bubbles generated on the chip surface merge into a very large secondary bubble that covers most of the chip surface. Therefore, it is reasonable to postulate that the primary bubbles cover on the pin finned surface in the present study. However, the bubbles accumulate in the channel and cover the heated surface easily at high heat fluxes in microgravity in the absence of buoyancy. Compared to chip S, a surface with higher CHF will lead to vapor accumulation in the channel severer. Therefore, the $CHF_{\mu g}/CHF_{1g}$ ratio of PF30-60 cannot reach a value as high as that of Chip S.

3.4. The effect of the factors on the $CHF_{\mu g}/CHF_{1g}$

It is well known that the inertial force and surface tension are the main factors for bubble departure in microgravity. This is because the capillary length L_c [$L_c = (\sigma/g(\rho_l - \rho_g))^{0.5}$], where σ is the surface tension, and ρ_l and ρ_g are the densities of the liquid and vapor phases, respectively, in microgravity is much larger than in normal gravity. Reinart et al. [53] conducted a two-phase-flow pressure-drop experiment on a space shuttle. Based on the results, they proposed that when the vapor Webber number, $We_g > 10$, the vapor inertia dominates rather than surface tension. Here, $We_g = \rho_g U_g^2 d/\sigma$, where d is the tube inner diameter and U_g is the vapor velocity. Moreover, based on the flow-pattern characteristics of gas-liquid two-phase flow in microgravity, Zhao et al. [54] proposed the Bond number and modified Froude number criteria for gravity independence in gas-liquid two-phase flow, and they pointed out that when $We_g > 0.8$–13, the vapor inertia dominates. Baba et al. [55] and Ohta and Baba [56] also proposed a new dominant force criteria based on the experimental data of one-component flow boiling, and the Weber number was defined as $We_m = \rho_m U_m^2 d/\sigma$, where d is the tube inner diameter, U_m the mean velocity, and ρ_m the mean density of liquid and vapor. They referenced the threshold of We_m as 5. Therefore, a large inlet velocity is necessary for overcoming the effects of the surface tension of bubble on flow boiling CHF. As we know, the Weber number, We [$We = \rho_l\rho_g V^2 D_h/(\rho_l + \rho_g)\sigma$], is a primary non-dimensional number that affects the bubble departure and heat transfer performance. Zhang et al. [57] found that the heater-length criterion ($We \geq 2\pi$) is dominant in microgravity for determination of the minimum flow velocity required to overcome all body force effects on flow boiling CHF. Fig. 14 shows the $CHF_{\mu g}/CHF_{1g}$ ratio under different inlet liquid velocities. The $CHF_{\mu g}/CHF_{1g}$ ratio is found to be very sensitive to the inlet velocity. However, different experimental conditions show obvious difference in $CHF_{\mu g}/CHF_{1g}$ values at the same inlet velocity, and the experimental condition also plays a very important role in $CHF_{\mu g}/CHF_{1g}$. Zhang et al. [34] found that the threshold of inlet velocity of inertial-force-dominant flow boiling ($CHF_{\mu g}/CHF_{1g} > 0.9$) is approximately 1.5 m/s in a single-side heated rectangular channel ($L \times w \times h$ = 101.6 mm × 2.5 mm × 5 mm). However, Konishi et al. [35] found the threshold of inlet velocity is approximately 1.0 m/s in an opposite double-side heated rectangular channel

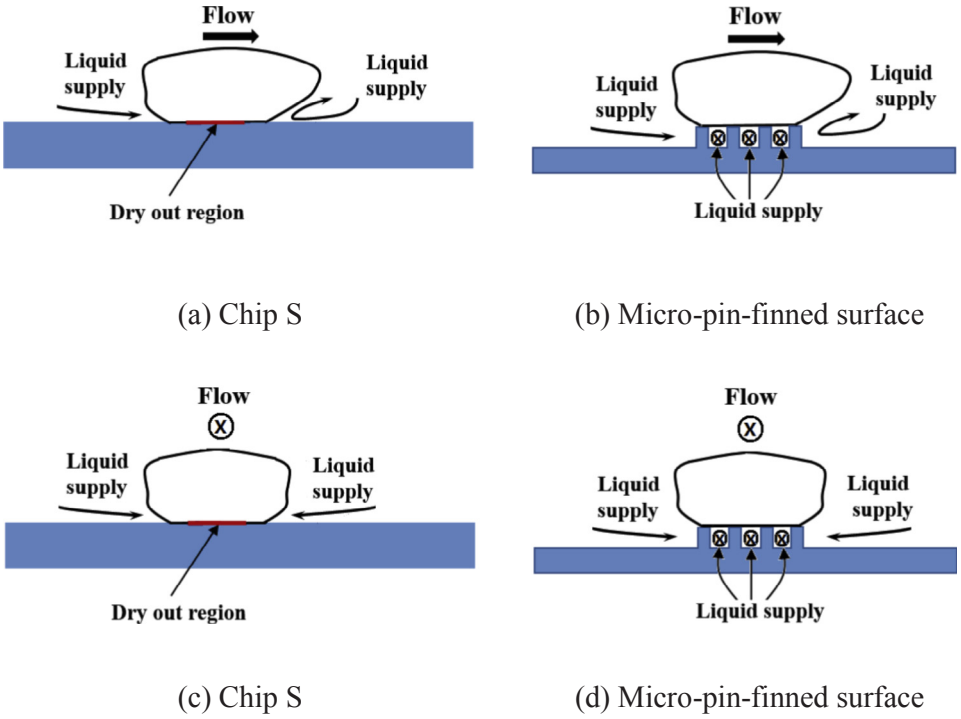

Fig. 13. Schematic diagram of liquid supply in high heat flux region.

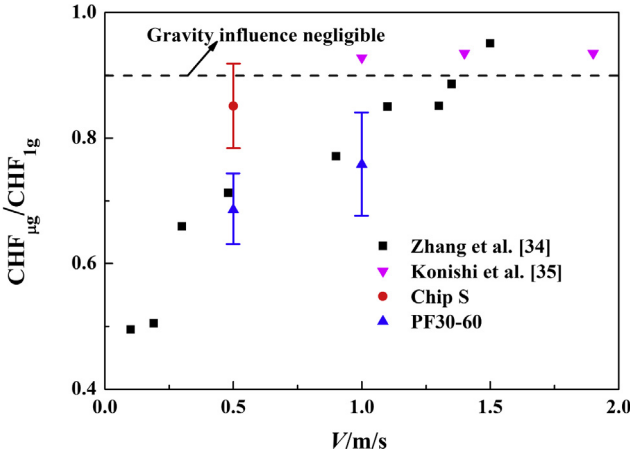

Fig. 14. The gravity influence on CHF with different channel geometry parameters and different surfaces.

($L \times w \times h = 114.6\,\text{mm} \times 2.5\,\text{mm} \times 5\,\text{mm}$). They found that double-sided heating with higher vapor production can lead to faster fluid motion. Moreover, the $CHF_{\mu g}/CHF_{1g}$ ratio of the smooth chip in this study is close to 0.9 at the inlet velocity $V = 0.5$ m/s. In addition, the $CHF_{\mu g}/CHF_{1g}$ ratio of PF30-60 is lower than that of Chip S at the same inlet velocity, because PF30-60 shows much higher CHF in normal gravity than that of Chip S. As analyzed in Section 3.3, the CHF of PF30-60 in microgravity cannot be enhanced as obviously as that in normal gravity compared with that of Chip S. Therefore, there are still other factors influencing the threshold inlet velocity of inertial-force-dominant flow boiling in microgravity, such as channel geometry and surface modification.

For a given heated surface and inlet velocity, the void fraction is a very important factor affecting heat transfer because it reflects the degree of bubble accumulation in the cross-section of the channel. A higher void fraction can result faster fluid motion and diminish the effects of the gravity level. However, it is impossible to obtain the exact value of void fraction in this study and in [34,35]. Therefore, from the viewpoint of vapor accumulation, we use a dimensionless channel number, *Ch*, to describe the influence of void fraction, and *Ch* can be obtained by channel-geometry parameters:

$$Ch = \frac{p_h}{p_w}\frac{1}{Eo}\frac{L}{L_c} = \frac{p_h L}{p_w h^2\sqrt{g(\rho_l-\rho_g)/\sigma}} \tag{8}$$

where p_h and p_w are the heated perimeter and wetted perimeter of the channel cross-section, respectively. *Eo* [$Eo = g(\rho_l - \rho_g)h^2/\sigma$] is the Eötvös number and g is the gravitational acceleration in microgravity (in this study, $g = 10^{-2}g_0$). A channel with larger *Ch* indicates serious accumulation of bubbles in the channel, weaker influence of gravity on CHF, and a value of the $CHF_{\mu g}/CHF_{1g}$ closer to 1. A channel with higher p_h/p_w has more severe bubble accumulation at the same heat flux and inlet velocity. Similarly, a channel with small *Eo* corresponds to the bubbles in the channel being confined and easily accumulated. In addition, a channel with large L/L_c promotes more bubble accumulation than a channel with small L/L_c.

For a given channel and inlet velocity, a modified surface with CHF enhancement in microgravity cannot be enhanced as obviously as that in microgravity. Moreover, it can be speculated that the $CHF_{\mu g}/CHF_{1g}$ ratio of a modified surface decreases with increasing ratio of the CHF of modified surface and the CHF of smooth surface in normal gravity ($CHF_{m,1g}/CHF_{ss,1g}$). A dimensionless surface number, $Sf = CHF_{ss,1g}/CHF_{m,1g}$, is proposed here to describe the effect of surface modification on the $CHF_{\mu g}/CHF_{1g}$ ratio. For a given channel and inlet velocity, the surface with lower *Sf* corresponds to more obvious CHF enhancement compared to the smooth surface, and the $CHF_{\mu g}/CHF_{1g}$ ratio is lower (see Table 3).

Combined with the dimensionless numbers *We*, *Ch* and *Sf*, the $CHF_{\mu g}/CHF_{1g}$ ratio can be predicted by considering the inertia force, surface tension, channel geometry and surface modification. Thus, the relationship of the $CHF_{\mu g}/CHF_{1g}$ ratio to these dimensionless numbers can be expressed as follows:

$$CHF_{\mu g}/CHF_{1g} = 0.179We^{0.325}Ch^{0.196}Sf^{2.568} + K \tag{9}$$

where K is the $CHF_{\mu g}/CHF_{1g}$ ratio at $V = 0$ m/s (pool boiling). In fact, the $CHF_{\mu g}/CHF_{1g}$ ratio at $V = 0.5$ m/s is also affected by the geometry of channel and surface modification. Therefore K can be expressed as follows:

$$K = 0.40Ch^{m}Sf^{n} \tag{10}$$

The constant 0.40 is the average $CHF_{\mu g}/CHF_{1g}$ ratio of unconfined pool boiling on the smooth surface at different gravity levels. The constant 0.40 is reasonable because most of the pool boiling experimental results indicated [39,58–63] that the value of the $CHF_{\mu g}/CHF_{1g}$ ratio is 0.31–0.53. The results of Xue et al. [40] and of Zhang et al. [41] revealed that the $CHF_{\mu g}/CHF_{1g}$ ratio of pool boiling in microgravity under unconfined conditions is influenced notably by surface modification and the $CHF_{\mu g}/CHF_{1g}$ ratio is increased obviously compared with the smooth surface. Through the experimental data in [40,41], the exponent n can be estimated as -0.64. However, there are no available $CHF_{\mu g}/CHF_{1g}$ data regarding confined pool boiling in microgravity. According to the results of confined-pool-boiling CHF [64–66], it can be found that the CHF under confined pool boiling is significantly lower than that under unconfined conditions. Although the influence of confinement is still unclear in microgravity, we can assume it has a similar influence on the $CHF_{\mu g}/CHF_{1g}$ ratio. The pool boiling confinement in a channel can also be described by the dimensionless number *Ch*. To fit the experimental data, we set the exponent of *Ch* to 0.05, and the $CHF_{\mu g}/CHF_{1g}$ ratio can be calculated using Eq. (11).

$$CHF_{\mu g}/CHF_{1g} = 0.179We^{0.325}Ch^{0.196}Sf^{2.568} + 0.40Ch^{0.05}Sf^{-0.64} \tag{11}$$

Fig. 15 shows the comparison of the predicted $CHF_{\mu g}/CHF_{1g}$ ratio calculated by the fitted correlation and experimental data. The predicted $CHF_{\mu g}/CHF_{1g}$ ratio is found to be in good agreement with the experimental data. This correlation provided a new perspective to find the threshold inlet velocity of inertia force dominant flow boiling at different gravity levels.

Table 3
Dimensionless numbers and parameters in the present study.

	V (m/s)	*We*	*Ch*	*Sf*	D_h (mm)	L_c (mm)	p_h (mm)	p_w (mm)	*h* (mm)	*L* (mm)
PF30-60	0.5	1.01	11.2	0.704	4.8	7.6	10	30	3	40
PF30-60	1.0	4.04	11.2	0.777	4.8	7.6	10	30	3	40
Chip S	0.5	1.01	11.2	1	4.8	7.6	10	30	3	40

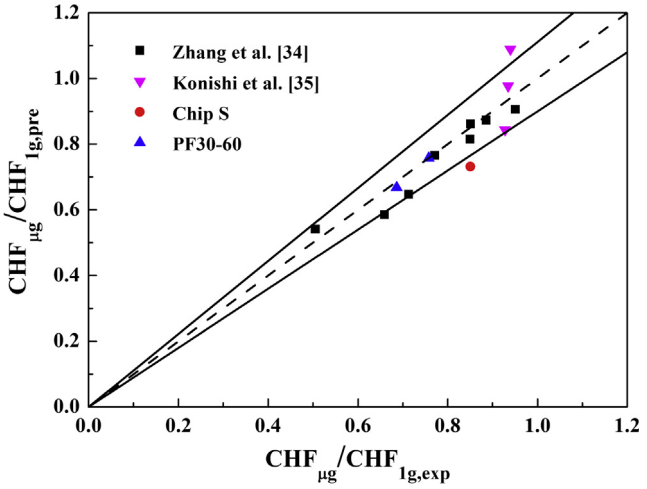

Fig. 15. Comparison of predicted $CHF_{\mu g}/CHF_{1g}$ ratio and experimental data.

4. Conclusions

In this study, the flow boiling heat transfer on the micro-pin-finned surface of subcooled air-dissolved FC-72 was investigated in normal gravity and microgravity. The factors affecting the value of $CHF_{\mu g}/CHF_{1g}$ ratio were investigated. The key findings from the study are concluded as follows:

(1) In the low and moderate heat fluxes regions, gravity has nearly no effects on the flow boiling heat transfer of the departure of the inertia force dominant bubbles. In contrast, in the high-heat-flux region, the flow boiling heat transfer deteriorates and the CHF decreases because of the lack of gravity. With increasing heat flux, bubbles cannot be swept away by shear flow, resulting in the deterioration of heat transfer and the decrease of CHF.
(2) In the high-heat-flux region, because the existence of micro-interconnected channels formed by micro-pin-fins leads to more convenient liquid supply than that of a smooth chip, the CHF of PF30-60 is slightly enhanced at the same inlet velocity.
(3) The gravity level affects CHF distinctly on PF30-60 compared with a smooth chip, although PF30-60 has better heat transfer performance.
(4) Under the present experimental conditions, CHF of micro-pin-finned surfaces deteriorate in microgravity. For PF30-60 at $V = 0.5$ m/s, the CHF point can be inferred to be between 20.8 and 24.5 W/cm^2, which is 63.0–74.2% of that in normal gravity. Regarding PF30-60 at $V = 1.0$ m/s, the CHF point can be inferred to be between 25.4 and 31.6 W/cm^2, which is 67.6–84.0% of that in normal gravity.

Acknowledgements

This work is supported by the project of National Natural Science Foundation of China (No. 51506169, No. 51636006, No. 51611130060), The Fundamental Research Funds For the Central Universities (No. cxtd2017004, xjj2017085), and the scientific research program for new lecturer of Xi'an Jiaotong University (No. DW010728K000000B), and China Postdoctoral Science Foundation funded project (No. 2015M582653), and the Postdoctoral Research Project of Shaanxi Province (No. 2016BSHEDZZ131).

References

[1] G.V. Rao, A.R. Balakrishnan, Heat transfer in nucleate pool boiling of multi-component mixtures, Exp. Therm Fluid Sci. 29 (1) (2005) 87–103.
[2] E. Salari, S.M. Peyghambarzadeh, M.M. Sarafraz, F. Hormozi, V. Nikkhah, Thermal behavior of aqueous iron oxide nano-fluid as a coolant on a flat disc heater under the pool boiling condition, Heat Mass Transf. 53 (1) (2016) 1–11.
[3] M.M. Sarafraz, F. Hormozi, Comparatively experimental study on the boiling thermal performance of metal oxide and multi-walled carbon nanotube nanofluids, Powder Technol. 287 (2016) 412–430.
[4] M.M. Sarafraz, F. Hormozi, Critical heat flux and pool boiling heat transfer analysis of synthesized zirconia aqueous nano-fluids, Int. Commun. Heat Mass Transf. 70 (4) (2016) 75–83.
[5] M.M. Sarafraz, F. Hormozi, S.M. Peyghambarzadeh, Pool boiling heat transfer to aqueous alumina nano-fluids on the plain and concentric circular micro-structured (CCM) surfaces, Exp. Therm Fluid Sci. 72 (2016) 125–139.
[6] M. Shojaeian, A. Koşar, Pool boiling and flow boiling on micro- and nanostructured surfaces, Exp. Therm Fluid Sci. 63 (2015) 45–73.
[7] N.S. Dhillon, J. Buongiorno, K.K. Varanasi, Critical heat flux maxima during boiling crisis on textured surfaces, Nat. Commun. 6 (2015) 8247.
[8] S.M.A.N.R. Abadi, J.P. Meyer, Numerical investigation into the inclination effect on conjugate pool boiling and the condensation of steam in a passive heat removal system, Int. J. Heat Mass Transf. (2017).
[9] G.R. Warrier, V.K. Dhir, D.F. Chao, Nucleate pool boiling eXperiment (NPBX) in microgravity: international space station, Int. J. Heat Mass Transf. 83 (2015) 781–798.
[10] X. Ma, P. Cheng, S. Gong, X. Quan, Mesoscale simulations of saturated pool boiling heat transfer under microgravity conditions, Int. J. Heat Mass Transf. 114 (2017) 453–457.
[11] P.D. Marco, W. Grassi, Effects of external electric field on pool boiling: Comparison of terrestrial and microgravity data in the ARIEL experiment, Exp. Therm Fluid Sci. 35 (5) (2011) 780–7877.
[12] R.E. Moehrle, J.N. Chung, Pool boiling heat transfer driven by an acoustic standing wave in terrestrial gravity and microgravity, Int. J. Heat Mass Transf. 93 (2016) 322–336.
[13] W. Lei, Z. Kang, F. Xie, M. Yuan, Y. Li, Prediction of pool boiling heat transfer for hydrogen in microgravity, Int. J. Heat Mass Transf. 94 (2016) 465–473.
[14] S. Takada, N. Kimura, M. Mamiya, H. Nagai, M. Murakami, Visualization study of growth of spherical bubble in He II boiling under microgravity condition, Phys. Procedia 67 (2015) 591–595.
[15] B.J. Qi, J.J. Wei, X.L. Wang, J.F. Zhao, Influences of wake-effects on bubble dynamics by utilizing micro-pin-finned surfaces under microgravity, Appl. Therm. Eng. 113 (2017) 1332–1344.
[16] P. Di Marco, Review of reduced gravity boiling heat transfer: European research, Therm. Eng. Microgravity 20 (4) (2003) 252–263.
[17] J. Kim, Review of reduced gravity boiling heat transfer: US research, Therm. Eng. Microgravity 20 (4) (2003) 264–271.
[18] H. Ohta, Review of reduced gravity boiling heat transfer: Japanese research, J. Jpn. Soc. Microgravity Appl. 20 (4) (2003) 272–285.
[19] J.F. Zhao, Two-phase flow and pool boiling heat transfer in microgravity, Int. J. Multiph. Flow 36 (2) (2010) 135–143.
[20] C. Colin, M. Narcy, P.E. Trejo, Flow boiling in pipe in microgravity, in: 13th International Conference on Heat Transfer, Fluid Mechanics and Thermodynamics, Portorož, Slovenia July 17–19, 2017.
[21] G.P. Celata, Flow boiling heat transfer in microgravity: recent results, Microgravity Sci. Technol. 19 (3–4) (2007) 13–17.
[22] Y. Ma, J.N. Chung, A study of bubble dynamics in reduced gravity forced-convection boiling, Int. J. Heat Mass Transf. 44 (2) (2001) 399–415.
[23] Y. Ma, J.N. Chung, An experimental study of forced convection boiling in microgravity, Int. J. Heat Mass Transf. 41 (15) (1998) 2371–2382.
[24] M. Saito, N. Yamaoka, K. Miyazaki, M. Kinoshita, Y. Abe, Boiling two-phase flow under microgravity, Nucl. Eng. Des. 146 (1) (1994) 451–461.
[25] G.P. Celata, M. Cumo, M. Gervasi, G. Zummo, Flow pattern analysis of flow boiling in microgravity, Multiphase Sci. Technol. 19 (2) (2007).
[26] M. Narcy, E.D. Malmazet, C. Colin, Flow boiling in tube under normal gravity and microgravity conditions, Int. J. Multiph. Flow 60 (2014) 50–63.
[27] W.R. Hu, J.F. Zhao, Slug to annular flow transition of microgravity two-phase flow, Int. J. Multiph. Flow 26 (2000) 1295–1304.
[28] J.F. Zhao, J.C. Xie, H. Lin, W.R. Hu, A.V. Ivanov, A.Yu. Belyaev, Experimental studies on two-phase flow patterns aboard Mir space station, Int. J. Multiph. Flow 27 (2001) 1931–1944.
[29] C. Baltis, G.P. Celata, M. Cumo, L. Saraceno, G. Zummo, Gravity influence on heat transfer rate in flow boiling, Microgravity Sci. Technol. 24 (3) (2012) 203–213.
[30] S. Luciani, D. Brutin, C. Le Niliot, O. Rahli, L. Tadrist, Flow boiling in minichannels under normal, hyper-, and microgravity: local heat transfer analysis using inverse methods, J. Heat Transf. 130 (10) (2008) 101502.
[31] S. Luciani, D. Brutin, C.L. Niliot, L. Tadrist, O. Rahli, Boiling heat transfer in a vertical microchannel: local estimation during flow boiling with a non intrusive method, Multiphase Sci. Technol. 21 (4) (2009).
[32] H. Ohta, Experiments on microgravity boiling heat transfer by using transparent heaters, Nucl. Eng. Des. 175 (1) (1997) 167–180.
[33] Y. Ma, J.N. Chung, An experimental study of critical heat flux (CHF) in microgravity forced-convection boiling, Int. J. Multiph. Flow 27 (10) (2001) 1753–1767.
[34] H. Zhang, I. Mudawar, M.M. Hasan, Flow boiling CHF in microgravity, Int. J. Heat Mass Transf. 48 (15) (2005) 3107–3118.
[35] C. Konishi, H. Lee, I. Mudawar, M.M. Hasan, H.K. Nahra, N.R. Hall, J.D. Wagner, R.L. May, J.R. Mackey, Flow boiling in microgravity: Part 2–Critical heat flux interfacial behavior, experimental data, and model, configurations, Int. J. Heat Mass Transf. 81 (2015) 721–736.
[36] C. Konishi, H. Lee, I. Mudawar, M.M. Hasan, H.K. Nahra, N.R. Hall, J.D. Wagner, R.L. May, J.R. Mackey, Flow boiling in microgravity: Part 1–Interfacial behavior and experimental heat transfer results, Int. J. Heat Mass Transf. 81 (2015) 705–720.

[37] C. Konishi, I. Mudawar, Review of flow boiling and critical heat flux in microgravity, Int. J. Heat Mass Transf. 80 (2015) 469–493.
[38] C. Baldassari, M. Marengo, Flow boiling in microchannels and microgravity, Prog. Energy Combust. Sci. 39 (1) (2013) 1–36.
[39] Y.F. Xue, J.F. Zhao, J.J. Wei, J. Li, D. Guo, S.X. Wan, Experimental study of nucleate pool boiling of fc-72 on smooth surface under microgravity, Microgravity Sci. Technol. 23 (Suppl. 1) (2011) S75–S85.
[40] Y.F. Xue, J.F. Zhao, J.J. Wei, Y.H. Zhang, B.J. Qi, Experimental study of nucleate pool boiling of FC-72 on micro-pin-finned surface under microgravity, Int. J. Heat Mass Transf. 63 (2013) 425–433.
[41] Y.H. Zhang, J.J. Wei, Y.F. Xue, X. Kong, J.F. Zhao, Bubble dynamics in nucleate pool boiling on micro-pin-finned surfaces in microgravity, Appl. Therm. Eng. 70 (1) (2014) 172–182.
[42] H. Honda, H. Takamastu, J.J. Wei, Enhanced boiling of FC-72 on silicon chips with micro-pin-fins and submicron-scale roughness, J. Heat Transf. 124 (2002) 383–390.
[43] J.J. Wei, H. Honda, Effects of fin geometry on boiling heat transfer from silicon chips with micro-pin-fins immersed in FC-72, Int. J. Heat Mass Transf. 46 (21) (2003) 4059–4070.
[44] J.J. Wei, H. Honda, Enhanced boiling heat transfer from electronic components by use of surface microstructures, Exp. Therm Fluid Sci. 28 (2004) 159–169.
[45] K.N. Rainey, G. Li, S.M. You, Flow boiling heat transfer from plain and microporous coated surfaces in subcooled FC-72, ASME J. Heat Transf. 123 (5) (2001) 918–925.
[46] W.R. Chang, C.A. Chen, J.H. Ke, T.F. Lin, Subcooled flow boiling heat transfer and associated bubble characteristics of FC-72 on a heated micro-pin-finned silicon chip, Int. J. Heat Mass Transf. 53 (2010) 5605–5621.
[47] J.P. O'Connor, S.M. You, A painting technique to enhance pool boiling heat transfer in FC-72, ASME J. Heat Transf. 117 (1995) 387–393.
[48] G.P. Celata, G. Zummo, Flow Boiling in Microgravity, EBECEM, Florianopolis, 2008.
[49] A.K. Sadaghiani, A. Koşar, Numerical and experimental investigation on the effects of diameter and length on high mass flux subcooled flow boiling in horizontal microtubes, Int. J. Heat Mass Transf. 92 (2016) 824–837.
[50] L. Sun, K. Mishima, An evaluation of prediction methods for saturated flow boiling heat transfer in mini-channels, Int. J. Heat Mass Transf. 52 (23) (2009) 5323–5329.
[51] I. Mudawar, D.E. Maddox, Critical heat flux in subcooled flow boiling of fluorocarbon liquid on a simulated electronic chip in a vertical rectangular channel, Int. J. Heat Mass Transf. 32 (2) (1989) 379–394.
[52] C.P. Tso, K.W. Tou, G.P. Xu, Flow boiling critical heat flux of FC-72 from flush-mounted and protruded simulated chips in a vertical rectangular channel, Int. J. Multiph. Flow 26 (3) (2000) 351–365.
[53] T. Reinarts, E. Ungar, C. Butler, Adiabatic two-phase pressure drop in microgravity – TEMP2A-3 flight experiment measurements and comparison with predictions, in: 33rd Aerospace Sciences Meeting and Exhibit, Reno, NV, Jan. 9–12, 1995.
[54] J.F. Zhao, J.C. Xie, H. Lin, W.R. Hu, A.V. Ivanov, A.Yu. Belyaev, Experimental study on gas/liquid two-phase flow in microgravity, in: 51st Int. Astronautical Cong., Rio de Janeiro, Brazil, Oct. 2–6, 2000.
[55] S. Baba, T. Sakai, K. Sawada, C. Kubota, Y. Wada, Y. Shinmoto, H. Ohta, H. Asano, O. Kawanami, K. Suzuki, Proposal of experimental setup on boiling two-phase flow on-orbit experiments onboard Japanese experiment module "KIBO", 2011, pp. 012055.
[56] H. Ohta, S. Baba, Boiling experiments under microgravity conditions, Exp. Heat Transf. 26 (2–3) (2013) 266–295.
[57] H. Zhang, I. Mudawar, M.M. Hasan, Application of flow boiling for thermal management of electronics in microgravity and reduced gravity space systems, in: Thermal and Thermomechanical Phenomena in Electronic Systems, 2008. ITHERM 2008. 11th Intersociety Conference on, IEEE, 2008, pp. 949–959.
[58] H.S. Lee, H. Merte, F. Chiaramonte, Pool boiling curve in microgravity, J. Thermophys. Heat Transf. 11 (2) (1997) 216–222.
[59] J. Kim, J.F. Benton, D. Wisniewski, Pool boiling heat transfer on small heaters: effect of gravity and subcooling, Int. J. Heat Mass Transf. 45 (19) (2002) 3919–3932.
[60] J.F. Zhao, J. Li, N. Yan, S.F. Wang, Bubble behavior and heat transfer in quasi-steady pool boiling in microgravity, Microgravity Sci. Technol. 21 (2009) 175–183.
[61] R. Raj, J. Kim, J. Mcquillen, Pool boiling heat transfer on the international space station: experimental results and model verification, J. Heat Transf.-Trans. ASME 134 (2012) 101504-101501-101514.
[62] M. Zell, J. Straub, A. Weinzierl, Nucleate pool boiling in subcooled liquid under microgravity results of Texus experimental investigations, in: 5th European Symp. on Material Science under Microgravity, 1984, pp. 327–333.
[63] T. Oka, Y. Abe, Y.H. Mori, A. Nagashima, Pool boiling heat transfer in microgravity (experiments with CFC-113 and water utilizing a drop shaft facility), JSME Int. J. Ser. B-Fluids Therm. Eng. 39 (4) (1996) 798–807.
[64] Y. Fujita, H. Ohta, S. Uchida, K. Nishikawa, Nucleate boiling heat transfer and critical heat flux in narrow space between rectangular surfaces, Int. J. Heat Mass Transf. 31 (2) (1988) 229–239.
[65] Y. Katto, S. Yokoya, K. Teraoka, Nucleate and transition boiling in a narrow space between two horizontal, parallel disk-surfaces, JSME Int. J. 20 (143) (2008) 638–643.
[66] M. Misale, G. Guglielmini, A. Priarone, HFE-7100 pool boiling heat transfer and critical heat flux in inclined narrow spaces, Int. J. Refrig. 32 (2) (2009) 235–245.